
This is an electronic reprint of the original article.
This reprint may differ from the original in pagination and typographic detail.

Ojanperä, A.; Havu, V.; Lehtovaara, Lauri; Puska, M.

Nonadiabatic Ehrenfest molecular dynamics within the projector augmented-wave method

Published in:
Journal of Chemical Physics

DOI:
[10.1063/1.3700800](https://doi.org/10.1063/1.3700800)

Published: 01/01/2012

Document Version
Publisher's PDF, also known as Version of record

Please cite the original version:
Ojanperä, A., Havu, V., Lehtovaara, L., & Puska, M. (2012). Nonadiabatic Ehrenfest molecular dynamics within the projector augmented-wave method. *Journal of Chemical Physics*, 136(14), 1-9. Article 144103.
<https://doi.org/10.1063/1.3700800>

This material is protected by copyright and other intellectual property rights, and duplication or sale of all or part of any of the repository collections is not permitted, except that material may be duplicated by you for your research use or educational purposes in electronic or print form. You must obtain permission for any other use. Electronic or print copies may not be offered, whether for sale or otherwise to anyone who is not an authorised user.

Nonadiabatic Ehrenfest molecular dynamics within the projector augmented-wave method

Ari Ojanperä, , Ville Havu, , Lauri Lehtovaara, and , and Martti Puska

Citation: *The Journal of Chemical Physics* **136**, 144103 (2012); doi: 10.1063/1.3700800

View online: <http://dx.doi.org/10.1063/1.3700800>

View Table of Contents: <http://aip.scitation.org/toc/jcp/136/14>

Published by the [American Institute of Physics](#)

Articles you may be interested in

[Perspective: Nonadiabatic dynamics theory](#)

The Journal of Chemical Physics **137**, 22A301 (2012); 10.1063/1.4757762

[On-the-fly ab initio molecular dynamics with multiconfigurational Ehrenfest method](#)

The Journal of Chemical Physics **137**, 22A506 (2012); 10.1063/1.4734313

[Ab initio Ehrenfest dynamics](#)

The Journal of Chemical Physics **123**, 084106 (2005); 10.1063/1.2008258

[Time-dependent density functional theory Ehrenfest dynamics: Collisions between atomic oxygen and graphite clusters](#)

The Journal of Chemical Physics **126**, 134307 (2007); 10.1063/1.2713391

COMPLETELY

REDESIGNED!



PHYSICS
TODAY

Physics Today Buyer's Guide
Search with a purpose.

Nonadiabatic Ehrenfest molecular dynamics within the projector augmented-wave method

Ari Ojanperä,¹ Ville Havu,¹ Lauri Lehtovaara,² and Martti Puska¹

¹Department of Applied Physics, Aalto University, P.O. Box 11100, FI-00076 Aalto, Finland

²LPMCN, Université Claude Bernard Lyon I, F69622 Villeurbanne Cedex, France

(Received 8 July 2011; accepted 20 March 2012; published online 10 April 2012)

We derive equations for nonadiabatic Ehrenfest molecular dynamics within the projector augmented-wave (PAW) formalism. The discretization of the electrons is time-dependent as the augmentation functions depend on the positions of the nuclei. We describe the implementation of the Ehrenfest molecular dynamics equations within the real-space PAW method. We demonstrate the applicability of our method by studying the vibration of NaCl, the torsional rotation of $\text{H}_2\text{C}=\text{NH}_2^+$ in both the adiabatic and the nonadiabatic regimes, and the hydrogen bombardment of $\text{C}_{40}\text{H}_{16}$. © 2012 American Institute of Physics. [<http://dx.doi.org/10.1063/1.3700800>]

I. INTRODUCTION

Many natural processes, such as light absorption, ignition of chemical reactions, and ion-atom collisions, are related to excited electronic states and their time development. The most general approach for treating such nonadiabatic processes, which in general involve two or more coupled electronic states, would be to solve the time-dependent many-body Schrödinger equation. However, this is not feasible for systems consisting of more than a few electrons. Moreover, the standard *ab initio* molecular dynamics methods such as Car-Parrinello MD (Ref. 1) or Born-Oppenheimer MD (BOMD) (see, for example, Ref. 2) confine electrons to a single adiabatic state, typically the ground state. Semiclassical methods, such as Ehrenfest molecular dynamics (Ehrenfest MD) or trajectory surface hopping³ (TSH), in which the electrons are treated quantum-mechanically via the time-dependent Schrödinger equation and the nuclei classically via the Newtonian mechanics, have been developed some decades ago, but only during the last decade they have become feasible in atomistic simulations beyond small systems. This is partly due to the methodological advances in time-dependent density functional theory⁴ (TDDFT) which provides a computationally affordable basis for the Ehrenfest MD and the TSH methods, and also due to the rapidly increasing amount of computational resources available. There are two realizations of TDDFT: the linear-response scheme,⁵ which is based on TD perturbation theory and the time propagation scheme, which is based on propagating the time-dependent Kohn-Sham (TDKS) equations.⁶ Ehrenfest MD is based on the real-time propagation scheme, while the linear-response scheme is better suited for TSH methods.

Ehrenfest MD within TDDFT offers a simple yet effective framework for simulating nonadiabatic processes by coupling the time-dependent Kohn-Sham equations⁶ with classical equations of motion for nuclei via the KS potential energy surface (PES). The method works well for condensed matter, where many single electron levels are involved and a single reaction path dominates the nonadiabatic process such as in carbon nanostructures. However, when reactions pass regions of

close lying electronic states but end up in a state which is well described by a single potential energy surface, TSH methods such as linear-response TDDFT-based implementation⁷ provide a more accurate description than the Ehrenfest MD. This is due to the deficiency of the Ehrenfest MD that the system remains in a mixed state after exiting the nonadiabatic region. Moreover, due to its mean-field character, the Ehrenfest MD cannot correctly describe multiple reaction paths.⁸ Especially when quantum-mechanical effects on the nuclei are important, one has to use methods that go beyond the semi-classical approximation such as *ab initio* multiple spawning⁹ (AIMS) or variational multi-configuration Gaussian wavepacket.¹⁰

The Ehrenfest MD has been successfully used for studying various nonadiabatic processes such as collisions between atomic oxygen and graphite clusters,¹¹ excited carrier dynamics in carbon nanotubes,¹² and electronic excitations in ion bombardment of carbon nanostructures.¹³ Previously, Ehrenfest MD has been implemented using the complete active space self-consistent field method¹⁴ as well as the TDDFT framework. For the TDDFT-based implementations, various basis sets such as LCAO,^{15–18} plane waves,¹⁹ and real-space grids²⁰ have been used. Real-space techniques have several advantages: (1) the quality of the results can be controlled by a single variable, the grid spacing, (2) parallelization can be done straightforwardly using domain decomposition, and (3) different boundary conditions such as Dirichlet, periodic, or a mixture of them can be easily applied.

In DFT-based electronic structure calculations, the projector augmented-wave (PAW) method²¹ is one of the most widely used methods for treating the problem of highly oscillatory wavefunctions near the nuclei. In spite of its extensive use, to our knowledge, it has not been used in Ehrenfest MD simulations previously. Compared to pseudopotentials, the PAW method improves the description of the transition metal elements and the first row elements with open *p*-shells. Moreover, the PAW method in real space allows one to use fewer grid points than pseudopotentials²² as well as longer time steps in the propagation of the TDKS equations.²³ The all-electron (AE) nature of the PAW method, even though the

core states are frozen, is also a methodological advantage over pseudopotentials. However, compared to pseudopotentials, Ehrenfest MD within the PAW method is more complicated due to the augmentation functions that depend on the atomic positions. First, an additional term describing the moving spatial gauge of the electrons must be included in the TDKS equations.²⁴ Also, the Hellmann-Feynman (HF) theorem (see, for example, Ref. 25), traditionally used for calculating the atomic forces with pseudopotentials, is no longer valid.

The present paper is constructed as follows. In Sec. II, we briefly describe the Ehrenfest MD equations within the Kohn-Sham formalism in a finite basis and our propagation algorithm for the coupled quantum-classical system. The Ehrenfest MD implementation within the PAW method is described in Sec. III. The applicability of our method is demonstrated in Sec. IV by carrying out simulations for NaCl, H₂C=NH₂⁺, and C₄₀H₁₆. Furthermore, the applicability of different forces in both the adiabatic and the nonadiabatic regimes is discussed. Finally, we give conclusive remarks in Sec. V.

II. EHRENFEST MD WITHIN THE KOHN-SHAM FORMALISM

A. Quantum-classical equations of motion

We consider a general time-dependent quantum-classical system within the Kohn-Sham formalism, in which the total energy of the electrons is defined as

$$E_{\text{el}}[\rho; \mathbf{R}] = T_s[\rho] + E_{\text{ext}}[\rho; \mathbf{R}] + E_{\text{H}}[\rho] + E_{\text{xc}}[\rho], \quad (1)$$

where T_s is the kinetic energy of the non-interacting electrons, E_{ext} is the energy due to the external potential, which in this case includes the electron-nucleus and nucleus-nucleus interactions, E_{H} is the Hartree energy, and E_{xc} is the exchange-correlation energy. The semicolon in Eq. (1) is used to distinguish between the function (electronic density ρ) and vector (atomic positions \mathbf{R}) dependencies of E_{el} . The corresponding Hamiltonian operator reads as (atomic units are used throughout the paper)

$$\hat{H} = -\frac{1}{2}\nabla^2 + V_{\text{ext}} + V_{\text{H}} + V_{\text{xc}}. \quad (2)$$

We expand the Kohn-Sham auxiliary wavefunctions ψ_n in terms of a basis $\{\chi_k\}$ that depends explicitly on the atomic positions,

$$\psi_n(\mathbf{r}, \mathbf{R}, t) = \sum_k c_{nk}(t)\chi_k(\mathbf{r}, \mathbf{R}). \quad (3)$$

Moreover, we assume that the time-dependency of the basis functions is solely due to the movement of the atomic positions. With this construction, we define the Hamiltonian matrix

$$H_{ij} = \langle \chi_i | \hat{H} | \chi_j \rangle. \quad (4)$$

The electronic subsystem is described by time-dependent Kohn-Sham equation,

$$i \frac{\partial \psi_n}{\partial t} = \hat{H} \psi_n. \quad (5)$$

Using the expansion of the wavefunctions given by Eq. (3), the above equation can be written as

$$i\mathbf{S} \frac{\partial \mathbf{c}_n}{\partial t} = (\mathbf{H} + \mathbf{P})\mathbf{c}_n, \quad (6)$$

where the vector \mathbf{c}_n contains the basis function coefficients of state n , c_{nk} , and we have introduced the matrices

$$S_{ij} = \langle \chi_i | \chi_j \rangle, \quad (7)$$

$$P_{ij} = -i \left\langle \chi_i \left| \frac{\partial \chi_j}{\partial t} \right. \right\rangle, \quad (8)$$

in addition to the Hamiltonian matrix \mathbf{H} . The \mathbf{S} matrix describes the overlap between the basis functions, while the \mathbf{P} matrix takes into account the moving spatial gauge of the electrons due to the changing atomic positions and conserves the norm of the electronic states. It disappears if the nuclei do not move. Furthermore, employing the chain rule, the \mathbf{P} matrix can be written in terms of the atomic velocities $\dot{\mathbf{R}}_a$ as

$$\mathbf{P} = -i \sum_a \dot{\mathbf{R}}_a \cdot \mathbf{D}_a, \quad (9)$$

with the definition

$$D_{a,ij} = \left\langle \chi_i \left| \frac{\partial \chi_j}{\partial \mathbf{R}_a} \right. \right\rangle. \quad (10)$$

The dynamics of the classical nuclei is described by the Newton equations of motion

$$M_a \ddot{\mathbf{R}}_a = \mathbf{F}_a, \quad (11)$$

where the force acting on the atom a , \mathbf{F}_a , is determined in Sec. II B.

B. Relations between different forces

The force on the classical nuclei is obtained by requiring that the total Hamiltonian of the quantum-classical system, usually interpreted as the total energy,

$$\mathcal{H} = \sum_a \frac{M_a}{2} \dot{\mathbf{R}}_a^2 + E_{\text{el}}, \quad (12)$$

be conserved.¹⁵ Thus, the energy-conserving (EC) force is the negative derivative of the electronic energy with respect to nuclear coordinates

$$\begin{aligned} \mathbf{F}_a^{\text{EC}} &= -\frac{dE_{\text{el}}}{d\mathbf{R}_a} \\ &= -\frac{\partial E_{\text{el}}}{\partial \mathbf{R}_a} - \sum_n \left[\frac{\partial E_{\text{el}}}{\partial \mathbf{c}_n} \frac{d\mathbf{c}_n}{d\mathbf{R}_a} + c.c. \right]. \end{aligned} \quad (13)$$

The energy gradient is given by

$$\frac{\partial E_{\text{el}}}{\partial \mathbf{c}_n^*} = f_n \mathbf{H} \mathbf{c}_n, \quad (14)$$

where f_n is the occupation number of state n . The derivatives of the coefficients \mathbf{c}_n can be calculated using the condition

$$\frac{d}{d\mathbf{R}_a} (\mathbf{c}_n^* \mathbf{S} \mathbf{c}_n) = 0, \quad (15)$$

and the relation between the matrix \mathbf{D}_a and the gradient of \mathbf{S}

$$\frac{\partial \mathbf{S}}{\partial \mathbf{R}_a} = \mathbf{D}_a + \mathbf{D}_a^*. \quad (16)$$

Consequently, we obtain the following expression for the energy-conserving force:

$$\mathbf{F}_a^{\text{EC}} = -\frac{\partial E_{\text{el}}}{\partial \mathbf{R}_a} + \sum_n f_n \mathbf{c}_n^* (\mathbf{H}\mathbf{S}^{-1} \mathbf{D}_a + c.c.) \mathbf{c}_n. \quad (17)$$

The time derivative of the total Hamiltonian reads as

$$\begin{aligned} \frac{d\mathcal{H}}{dt} &= \sum_a \dot{\mathbf{R}}_a \cdot \mathbf{F}_a + \frac{dE_{\text{el}}}{dt} \\ &= \sum_a \dot{\mathbf{R}}_a \cdot \left[\mathbf{F}_a + \frac{\partial E_{\text{el}}}{\partial \mathbf{R}_a} \right. \\ &\quad \left. - \sum_n f_n \mathbf{c}_n^* (\mathbf{H}\mathbf{S}^{-1} \mathbf{D}_a + c.c.) \mathbf{c}_n \right]. \end{aligned} \quad (18)$$

Clearly, when we insert the EC force into Eq. (18), the first term inside the brackets cancels out the other terms, and hence the time derivative equals zero.

At this point, we note that the definition of the force based on total energy conservation is not unique. The most general force for quantum-classical MD is obtained by requiring that the quantum-classical action be stationary.^{16,18} In the Kohn-Sham formalism, the action can be written as a sum of the classical action \mathcal{A}_c and the quantum-mechanical action \mathcal{A}_q ,

$$\begin{aligned} \mathcal{A} &= \mathcal{A}_c + \mathcal{A}_q = \int_{t_0}^{t_1} \left[\sum_a \frac{M_a}{2} \dot{\mathbf{R}}_a^2 \right] dt \\ &\quad + \int_{t_0}^{t_1} \left[\sum_n f_n \langle \psi_n | i \frac{\partial}{\partial t} - \frac{\nabla^2}{2} | \psi_n \rangle \right] dt - \mathcal{A}_{\text{pot}}, \end{aligned} \quad (19)$$

where the potential part \mathcal{A}_{pot} includes the external and Hartree energies and the exchange-correlation action \mathcal{A}_{xc} ,

$$\begin{aligned} \mathcal{A}_{\text{pot}} &= \int_{t_0}^{t_1} (E_{\text{ext}} + E_{\text{H}}) dt + \mathcal{A}_{\text{xc}} \\ &= \int_{t_0}^{t_1} \int \rho(\mathbf{r}, \mathbf{R}, t) \left[V_{\text{ext}}(\mathbf{r}, \mathbf{R}) \right. \\ &\quad \left. + \frac{1}{2} \int \frac{\rho(\mathbf{r}', \mathbf{R}, t)}{|\mathbf{r} - \mathbf{r}'|} d\mathbf{r}' \right] d\mathbf{r} dt + \mathcal{A}_{\text{xc}}. \end{aligned} \quad (20)$$

By making the total action stationary, one actually obtains additional velocity-dependent terms in the forces as shown in Ref. 16. In Sec. III B, we discuss this further and present the additional force terms in the PAW method.

In order to see the connection to the ground state Pulay force,²⁶ we note that if the electronic subsystem remains in its ground state,

$$\mathbf{H}\mathbf{c}_n = \epsilon_n \mathbf{S}\mathbf{c}_n, \quad (21)$$

the EC force reduces to the well-known form of Hellmann-Feynman force plus Pulay corrections (see, for example, Ref. 2), which we in this context call the incomplete basis

set corrected (IBSC) force,

$$\mathbf{F}_a^{\text{IBSC}} = -\frac{\partial E_{\text{el}}}{\partial \mathbf{R}_a} + \sum_n f_n \epsilon_n \mathbf{c}_n^* \frac{\partial \mathbf{S}}{\partial \mathbf{R}_a} \mathbf{c}_n. \quad (22)$$

The Pulay force in Eq. (22) constitutes of the second term on the right-hand side and the terms containing the matrix elements $\langle \frac{\partial \chi_i}{\partial \mathbf{R}_a} | \hat{H} | \chi_j \rangle + \langle \chi_i | \hat{H} | \frac{\partial \chi_j}{\partial \mathbf{R}_a} \rangle$. In the case of nonadiabatic processes, the ground state assumption [Eq. (21)] might yield inadequate results in terms of the total energy conservation.

C. Time propagation of the electron-ion system

In order to carry out actual simulations, a propagation algorithm for the quantum-classical system [Eqs. (6) and (11)] is required. First, we use the following splitting for the propagation of coupled electrons and ions:

$$\begin{aligned} U_{N,e}(t + \Delta t, t) &= U_N \left(t + \frac{\Delta t}{2}, t \right) U_e(t + \Delta t, t) \\ &\quad \times U_N \left(t + \Delta t, t + \frac{\Delta t}{2} \right) + \mathcal{O}(\Delta t^3), \end{aligned} \quad (23)$$

where the propagator for the nuclei, U_N , is the standard velocity Verlet,²⁷ while the electronic states (U_e) are propagated using the so-called semi-implicit Crank Nicholson (SICN) method.^{22,28} The idea of the method is to first approximate the Hamiltonian matrix \mathbf{H} to be constant during the time step and solve the following linear equation to obtain the predicted future electronic states $\mathbf{c}_n^{\text{pred}}$

$$\begin{aligned} \left[\mathbf{S} + i \frac{\Delta t}{2} (\mathbf{H}(t) + \mathbf{P}) \right] \mathbf{c}_n^{\text{pred}}(t + \Delta t) \\ = \left[\mathbf{S} - i \frac{\Delta t}{2} (\mathbf{H}(t) + \mathbf{P}) \right] \mathbf{c}_n(t) + \mathcal{O}(\Delta t^2). \end{aligned} \quad (24)$$

Then, the predicted future Hamiltonian matrix, based on $\mathbf{c}_n^{\text{pred}}$, is used for calculating the Hamiltonian matrix in the middle of the time step, $\mathbf{H}(t + \Delta t/2) = \frac{1}{2}(\mathbf{H}(t) + \mathbf{H}^{\text{pred}}(t + \Delta t)) + \mathcal{O}(\Delta t^2)$. Now, using the notation $\mathbf{H}_{1/2} = \mathbf{H}(t + \Delta t/2)$, the final, propagated states $\mathbf{c}_n(t + \Delta t)$ can be obtained from

$$\begin{aligned} \left[\mathbf{S} + i \frac{\Delta t}{2} (\mathbf{H}_{1/2} + \mathbf{P}) \right] \mathbf{c}_n(t + \Delta t) \\ = \left[\mathbf{S} - i \frac{\Delta t}{2} (\mathbf{H}_{1/2} + \mathbf{P}) \right] \mathbf{c}_n(t) + \mathcal{O}(\Delta t^3). \end{aligned} \quad (25)$$

In the supplementary material,²⁹ we study the total energy conservation of a one-dimensional test system in a position-dependent basis. We compare the HF, IBSC, and EC forces and discuss their applicability in adiabatic and nonadiabatic regimes.

III. EHRENFEST MD WITHIN THE PAW FORMALISM

The central idea of the PAW method is that the all-electron wavefunctions can be reconstructed from the pseudo-wavefunctions by adding the all-electron part and subtracting the pseudo part inside augmentation spheres defined for each atom. The method is based on the following linear transformation between the KS pseudo ($\tilde{\psi}_n$) and all-electron (ψ_n)

wavefunctions:

$$\psi_n = \hat{T} \tilde{\psi}_n = \left[1 + \sum_{a,i} (|\phi_i^a\rangle - |\tilde{\phi}_i^a\rangle) \langle \tilde{p}_i^a | \right] \tilde{\psi}_n, \quad (26)$$

where i is a multi-index consisting of the quantum numbers l , m , and n , \tilde{p}_i^a are the projectors, \hat{T} is the PAW transformation operator, and $\tilde{\phi}_i^a$ and ϕ_i^a are the pseudo and AE partial waves, respectively. With this construction, all observables in the PAW method consist of a smooth part and atomic corrections, for example, the PAW total energy for electrons reads as

$$E_{\text{el}}^{\text{PAW}} = \tilde{E} + \sum_a (E_a - \tilde{E}_a), \quad (27)$$

where the expressions for the different terms and a detailed description of the real-space PAW method are given in Ref. 30.

Ehrenfest MD within the PAW formalism resembles the finite basis formalism presented in Sec. II. The first notable difference is that within the PAW method, we actually have a basis defined by two different functions, the projectors \tilde{p}_i^a and the pseudo-partial waves $\tilde{\phi}_i^a$, which fulfill

$$\langle \tilde{p}_{i_1}^a | \tilde{\phi}_{i_2}^a \rangle = \delta_{i_1, i_2}. \quad (28)$$

The second notable difference is that the dependency on the atomic positions arises from the position-dependent PAW transformation operator \hat{T} . As in Sec. II, there appears an additional term due to the moving basis set in the TDKS equation [Eq. (5)].

A. Electron dynamics

We start from the all-electron TDKS equation [Eq. (5)] by applying the PAW transformation [Eq. (26)]. Then, the TDKS equation is operated from the left by the adjoint of the PAW transformation operator, \hat{T}^\dagger . Subsequently, we arrive at the following PAW-transformed TDKS equation:

$$i \tilde{S} \frac{\partial \tilde{\psi}_n}{\partial t} = (\tilde{H} + \tilde{P}) \tilde{\psi}_n, \quad (29)$$

where $\tilde{S} = \hat{T}^\dagger \hat{T}$ is the PAW overlap operator, and $\tilde{H} = \hat{T}^\dagger \hat{H} \hat{T}$ is the PAW Hamiltonian operator. The \tilde{P} term, which corresponds to the \mathbf{P} matrix presented in Sec. II A, reads as

$$\tilde{P} = -i \hat{T}^\dagger \frac{\partial \hat{T}}{\partial t}. \quad (30)$$

It takes into account the time evolution of the PAW transformation operator in TDDFT-based quantum-classical MD simulations. Qian *et al.*²⁴ derived the following expression for this term:

$$\begin{aligned} \tilde{P} &= -i \sum_a \mathbf{R}_a \cdot (1 + \hat{t}_a^\dagger) \frac{\partial}{\partial \mathbf{R}_a} (1 + \hat{t}_a) \\ &= -i \sum_a \mathbf{R}_a \cdot \hat{\mathbf{D}}_a, \end{aligned} \quad (31)$$

where $\hat{t}_a = \sum_i (|\phi_i^a\rangle - |\tilde{\phi}_i^a\rangle) \langle \tilde{p}_i^a |$ is a projection operator belonging to atom a , and we have defined the operator $\hat{\mathbf{D}}_a$ in the spirit of the formalism presented in Sec. II. Moreover,

Eq. (31) only holds if the overlap between the PAW augmentation spheres is zero. In practice, however, Eq. (31) turns out to work well even in the case of overlapping augmentation spheres as long the overlap is not significant. The operator $\hat{\mathbf{D}}_a$ can be written in the following form [Appendix]:

$$\begin{aligned} \hat{\mathbf{D}}_a &= \sum_{i_1, i_2} \left[|\tilde{p}_{i_1}^a\rangle O_{i_1, i_2}^a \left\langle \frac{\partial \tilde{p}_{i_2}^a}{\partial \mathbf{R}_a} \right| \right. \\ &\quad \left. + |\tilde{p}_{i_1}^a\rangle \left(\left\langle \phi_{i_1}^a \left| \frac{\partial \phi_{i_2}^a}{\partial \mathbf{R}_a} \right\rangle - \left\langle \tilde{\phi}_{i_1}^a \left| \frac{\partial \tilde{\phi}_{i_2}^a}{\partial \mathbf{R}_a} \right\rangle \right) \langle \tilde{p}_{i_2}^a | \right]. \end{aligned} \quad (32)$$

The matrix elements O_{i_1, i_2}^a describe the overlap between the all-electron and pseudo-partial waves

$$O_{i_1, i_2}^a = \langle \phi_{i_1}^a | \phi_{i_2}^a \rangle - \langle \tilde{\phi}_{i_1}^a | \tilde{\phi}_{i_2}^a \rangle. \quad (33)$$

B. Atomic forces

The next task is to derive an expression for the Ehrenfest force. The total energy of the quantum-classical system reads within the PAW method as

$$E_{\text{tot}} = \sum_a \frac{M_a}{2} \mathbf{R}_a^2 + E_{\text{el}}^{\text{PAW}}, \quad (34)$$

where the nucleus-nucleus interaction is included in the electronic energy. Using the same reasoning as in Sec. II B, i.e., the conservation of the total energy, we calculate the force as the negative derivative of the electronic energy,

$$\begin{aligned} \mathbf{F}_a^{\text{EC}} &= -\frac{dE_{\text{el}}^{\text{PAW}}}{d\mathbf{R}_a} \\ &= -\frac{\partial E_{\text{el}}^{\text{PAW}}}{\partial \mathbf{R}_a} - \sum_n \left[\frac{\partial E_{\text{el}}^{\text{PAW}}}{\partial \tilde{\psi}_n} \frac{d\tilde{\psi}_n}{d\mathbf{R}_a} + c.c. \right] \\ &= -\frac{\partial E_{\text{el}}^{\text{PAW}}}{\partial \mathbf{R}_a} + \sum_n f_n \langle \tilde{\psi}_n | \hat{\mathbf{D}}_a^\dagger \tilde{S}^{-1} \tilde{H} + c.c. | \tilde{\psi}_n \rangle. \end{aligned} \quad (35)$$

By defining $\tilde{g}_n = \tilde{S}^{-1} \tilde{H} \tilde{\psi}_n$ and the vector-valued matrix elements

$$\mathbf{\Delta}_{i_1, i_2}^a = \left\langle \phi_{i_1}^a \left| \frac{\partial \phi_{i_2}^a}{\partial \mathbf{R}_a} \right\rangle - \left\langle \tilde{\phi}_{i_1}^a \left| \frac{\partial \tilde{\phi}_{i_2}^a}{\partial \mathbf{R}_a} \right\rangle, \quad (36)$$

the following relation can be used to calculate the second term on the right-hand side of Eq. (35):

$$\begin{aligned} \langle \tilde{\psi}_n | \hat{\mathbf{D}}_a^\dagger \tilde{S}^{-1} \tilde{H} | \tilde{\psi}_n \rangle &= \sum_{i_1, i_2} \left[\left\langle \tilde{\psi}_n \left| \frac{\partial \tilde{p}_{i_2}^a}{\partial \mathbf{R}_a} \right\rangle O_{i_1, i_2}^a \langle \tilde{p}_{i_1}^a | \tilde{g}_n \rangle \right. \\ &\quad \left. + \langle \tilde{\psi}_n | \tilde{p}_{i_2}^a \rangle \mathbf{\Delta}_{i_1, i_2}^a \langle \tilde{p}_{i_1}^a | \tilde{g}_n \rangle \right]. \end{aligned} \quad (37)$$

With this expression, the EC force can be straightforwardly implemented. The matrix elements O_{i_1, i_2}^a and $\mathbf{\Delta}_{i_1, i_2}^a$ are calculated on radial grids inside the PAW augmentation spheres, whereas the terms involving the pseudo-wavefunctions are computed on uniform Cartesian grids.

In a similar fashion as in Sec. II B, the EC force reduces to a Pulay-like ground state expression by assuming

$$\tilde{H} \tilde{\psi}_n = \epsilon_n \tilde{S} \tilde{\psi}_n. \quad (38)$$

Consequently, the IBSC force within the PAW method is

$$\mathbf{F}_a^{\text{IBSC}} = -\frac{\partial E_{\text{el}}^{\text{PAW}}}{\partial \mathbf{R}_a} + \sum_n f_n \epsilon_n \langle \tilde{\psi}_n | \frac{\partial \tilde{S}}{\partial \mathbf{R}_a} | \tilde{\psi}_n \rangle. \quad (39)$$

This force is used for ground state calculations in the GPAW package.^{30,31}

At this point, we return to the discussion of the definition of forces in Sec II B. First, we rewrite the quantum-mechanical action [Eq. (19)] using the very widely used adiabatic approximation for the exchange-correlation part,³²

$$\mathcal{A}_{\text{xc}}[\rho] = \int_{t_0}^{t_1} E_{\text{xc}}[\rho] |_{\rho=\rho(\mathbf{r},t)} dt. \quad (40)$$

Now, the quantum-mechanical action [Eq. (19)] can be written in terms of the Kohn-Sham energy,

$$\mathcal{A}_q = \int_{t_0}^{t_1} \left[\sum_n f_n \langle \psi_n | i \frac{\partial}{\partial t} | \psi_n \rangle - E_{\text{el}} \right] dt. \quad (41)$$

The PAW action, then, can be obtained by replacing E_{el} with the corresponding PAW expression for the total energy, $E_{\text{el}}^{\text{PAW}}$. Moreover, applying the PAW transformation to the first term inside the brackets in Eq. (41) gives

$$\begin{aligned} \mathcal{A}_q &= \int_{t_0}^{t_1} \mathcal{L}_q dt \\ &= \int_{t_0}^{t_1} \left[\sum_n f_n \langle \tilde{\psi}_n | \hat{T}^\dagger \left(i \frac{\partial}{\partial t} \right) \hat{T} | \tilde{\psi}_n \rangle - E_{\text{el}}^{\text{PAW}} \right] dt. \end{aligned} \quad (42)$$

Expanding the functional \mathcal{L}_q gives

$$\begin{aligned} \mathcal{L}_q &= \sum_n f_n \left[\langle \tilde{\psi}_n | i \sum_b \dot{\mathbf{R}}_b \cdot \hat{\mathbf{D}}_b | \tilde{\psi}_n \rangle \right. \\ &\quad \left. + i \langle \tilde{\psi}_n | \tilde{S} | \frac{\partial \tilde{\psi}_n}{\partial t} \rangle \right] - E_{\text{el}}^{\text{PAW}}. \end{aligned} \quad (43)$$

The force acting on atom a is obtained by requiring that the variation of the total action with respect to the position of that atom vanishes,

$$\frac{\delta \mathcal{A}}{\delta \mathbf{R}_a} = \frac{\delta \mathcal{A}_c}{\delta \mathbf{R}_a} + \frac{\partial \mathcal{L}_q}{\partial \mathbf{R}_a} - \frac{d}{dt} \frac{\partial \mathcal{L}_q}{\partial \dot{\mathbf{R}}_a} = 0. \quad (44)$$

The contribution from the classical action is just $\delta \mathcal{A}_c / \delta \mathbf{R}_a = -M_a \dot{\mathbf{R}}_a$. According to Eq. (44) and Newton's second law, the force is then obtained by varying the quantum-mechanical part. This gives

$$\begin{aligned} \frac{\delta \mathcal{A}_q}{\delta \mathbf{R}_a} &= -\frac{\partial E_{\text{el}}^{\text{PAW}}}{\partial \mathbf{R}_a} + \sum_n f_n \left[\langle \tilde{\psi}_n | \hat{\mathbf{D}}_a^\dagger \tilde{S}^{-1} \tilde{H} + c.c. | \tilde{\psi}_n \rangle \right. \\ &\quad \left. + \langle \tilde{\psi}_n | \hat{\mathbf{D}}_a^\dagger \tilde{S}^{-1} \tilde{P} + c.c. | \tilde{\psi}_n \rangle \right. \\ &\quad \left. - i \langle \tilde{\psi}_n | \frac{d\hat{T}^\dagger}{dt} \frac{\partial \hat{T}}{\partial \mathbf{R}_a} | \tilde{\psi}_n \rangle + i \langle \tilde{\psi}_n | \frac{\partial \hat{T}^\dagger}{\partial \mathbf{R}_a} \frac{d\hat{T}}{dt} | \tilde{\psi}_n \rangle \right]. \end{aligned} \quad (45)$$

We can immediately recognize that this expression contains the EC force [Eq. (35)] plus additional terms,

$$\frac{\delta \mathcal{A}_q}{\delta \mathbf{R}_a} = \mathbf{F}_a^{\text{EC}} + \mathbf{F}_a^{\text{TD}}. \quad (46)$$

The correction term \mathbf{F}_a^{TD} can be further expanded using the chain rule and assuming zero overlap between the augmentation spheres of different atoms,

$$\mathbf{F}_a^{\text{TD}} = i \sum_n f_n \langle \tilde{\psi}_n | \hat{\mathbf{C}}_a | \tilde{\psi}_n \rangle, \quad (47)$$

where the operator $\hat{\mathbf{C}}_a$ reads as

$$\begin{aligned} \hat{\mathbf{C}}_a &= (\dot{\mathbf{R}}_a \cdot \hat{\mathbf{D}}_a^\dagger) \tilde{S}^{-1} \hat{\mathbf{D}}_a - \hat{\mathbf{D}}_a^\dagger \tilde{S}^{-1} (\dot{\mathbf{R}}_a \cdot \hat{\mathbf{D}}_a) \\ &\quad + \frac{\partial \hat{T}^\dagger}{\partial \mathbf{R}_a} \left(\dot{\mathbf{R}}_a \cdot \frac{\partial \hat{T}}{\partial \mathbf{R}_a} \right) - \left(\dot{\mathbf{R}}_a \cdot \frac{\partial \hat{T}^\dagger}{\partial \mathbf{R}_a} \right) \frac{\partial \hat{T}}{\partial \mathbf{R}_a}. \end{aligned} \quad (48)$$

These velocity-dependent terms resemble the additional terms presented in Ref. 16, but the terms with different atom indices are now zero due to the zero overlap of augmentation functions of different atoms. The purpose of the force correction [Eq. (47)] is to guarantee momentum balance.¹⁶ However, the implementation of the operator $\hat{\mathbf{C}}_a$ [Eq. (48)] is not trivial in the real-space PAW method. Moreover, the energy-conserving force approach has been successfully applied to a variety of problems in earlier localized basis set work (see Ref. 15 and references therein). Therefore, we use the EC force in the present implementation and leave the implementation of the extra terms arising from making the quantum-classical action stationary as future work.

The coupled electron-ion system is propagated using the combination of SICN and the velocity Verlet algorithm as presented in Sec. II C.

C. Inverse overlap operator

The only remaining task is the calculation of the inverse PAW overlap operator \tilde{S}^{-1} . We use two different approaches for this. In the first approach, we assume that the inverse overlap operator can be written as

$$\tilde{S}^{-1} = 1 + \sum_a \sum_{i_1, i_2} |\tilde{p}_{i_1}^a\rangle C_{i_1, i_2}^a |\tilde{p}_{i_2}^a\rangle, \quad (49)$$

where C_{i_1, i_2}^a are the inverse overlap coefficients. They can be obtained from the linear equation resulting from the requirement

$$\tilde{S}^{-1} \tilde{S} = 1, \quad (50)$$

in which we also assume that there is no overlap between the PAW augmentation spheres. For this reason, this approach will likely produce unsatisfactory results if the overlap is non-zero. In the second approach, we obtain the required $\tilde{S}^{-1} \tilde{H} \tilde{\psi}_n$ terms by solving the linear equations

$$\tilde{S} \tilde{x} = \tilde{H} \tilde{\psi}_n, \quad (51)$$

iteratively using the conjugate gradient (CG) method. This approach is generally more accurate than the approximative inverse method [Eqs. (49) and (50)] and less sensitive to PAW overlap and numerical errors due to a large grid spacing. Table I shows that the approximative inverse method is very

sensitive to the grid spacing used in the calculations. However, the CG method will likely consume more computational resources than the approximative method.

IV. CALCULATIONS FOR SMALL AND MEDIUM-SIZED MOLECULES

In order to test our PAW-based Ehrenfest MD method, we study the dynamics of small and medium-sized molecules both in adiabatic and in nonadiabatic cases. The adiabatic cases include the vibration of the NaCl molecule, and the rotation of the $\text{H}_2\text{C}=\text{NH}_2^+$ molecule about its internal axis with a small initial kinetic energy. Nonadiabatic effects, then, are studied in the case of $\text{H}_2\text{C}=\text{NH}_2^+$ with a high initial kinetic energy, and also in the hydrogen bombardment of the $\text{C}_{40}\text{H}_{16}$ molecule. We use the local-density approximation exchange-correlation functional³³ in all the calculations. The grid spacing is $h = 0.2 \text{ \AA}$ unless specified otherwise.

A. Vibration of the NaCl molecule

First, we study the total energy conservation of the NaCl molecule. The simulations begin from equilibrium, $d_{\text{eq}} = 2.36 \text{ \AA}$, with an initial kinetic energy of 2 eV. The period of the NaCl vibration calculated with the BOMD is $T_{\text{BOMD}} = 181.6 \text{ fs}$. With this low initial kinetic energy, the vibration is almost adiabatic, and subsequently the period obtained with the Ehrenfest MD ($\Delta t = 8 \text{ as}$, IBSC force) is very close to the BOMD result, $T_{\text{EF}} = 181.4 \text{ fs}$. This is not surprising as the Ehrenfest MD should reduce to the BOMD in the case of adiabatic processes. We investigate the difference between the IBSC and EC forces in terms of the total energy conservation, using both the approximative and the CG inverse method for calculating the inverse overlap operator. The decay of the error in the total energy as a function of the simulation time step is shown in Fig. 1. For time steps below 10 as, there is little difference between the IBSC and EC forces. Actually the total energy error with the IBSC force is slightly smaller than that with the EC force, thus rendering the EC force unnecessary in this adiabatic case. Moreover, the two methods used for calculating the inverse overlap operator give practically identical results.

B. Rotation of the $\text{H}_2\text{C}=\text{NH}_2^+$ molecule

Next, we turn our attention to simulating nonadiabatic dynamics. The dynamics of the $\text{H}_2\text{C}=\text{NH}_2^+$ molecule has been studied with both the Hartree-Fock-based Ehrenfest dynamics³⁴ and the trajectory surface hopping method.⁷ We study the torsional rotation of the molecule about its internal axis by carrying out Ehrenfest MD calculations with two different initial torsional kinetic energies, $E_k = 1.5 \text{ eV}$ and $E_k = 10 \text{ eV}$. In order to investigate the nonadiabaticity in our simulations, we also carry out PAW-based BOMD calculations for both initial kinetic energies. Based on the results presented in Ref. 34, the rotation is expected to be adiabatic with $E_k = 1.5 \text{ eV}$, whereas with $E_k = 10 \text{ eV}$ we expect the Ehren-

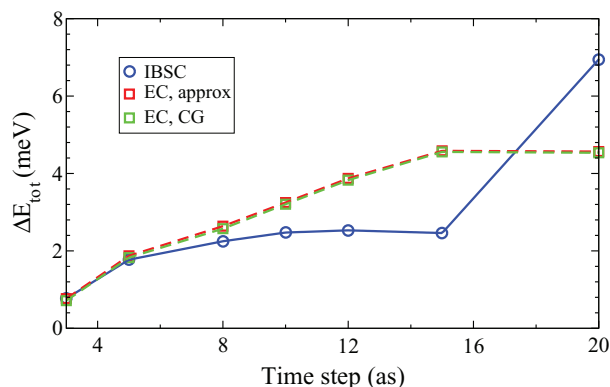


FIG. 1. Decay of the error in the total energy of the NaCl molecule as a function of the simulation time step. The results are shown for the IBSC and the EC forces [Eqs. (39) and (35), respectively]. Approx denotes the approximative method for calculating the inverse overlap operator [Eqs. (49) and (50)], and CG corresponds to the conjugate gradient method. The lines are just a guide to the eye.

fest MD results to clearly differ from the BOMD results. The molecule is initially in the planar equilibrium geometry. For both initial kinetic energies, we carry out calculations using two different time steps, $\Delta t = 2$ and 5 as. Similar to the calculations for the NaCl molecule, the IBSC and the EC forces are applied. In the case of the EC force, both the approximative and the CG method are used for computing the inverse overlap operator.

The potential energy surfaces obtained from the Ehrenfest MD and the BOMD simulations for both initial kinetic energies are presented in Fig. 2. For the Ehrenfest PES, the EC force in conjunction with the CG method for calculating \hat{S}^{-1} is used.

The figure illustrates that the dynamics is nearly adiabatic with $E_k = 1.5 \text{ eV}$ as the Ehrenfest and the Born-Oppenheimer PES are almost identical. In contrast, with $E_k = 10 \text{ eV}$, the Ehrenfest PES starts to deviate rapidly from the BO one, which indicates a significant amount of nonadiabaticity in the dynamics.

In the adiabatic case, the total energy is conserved to a few meV even with the IBSC force. With $E_k = 10 \text{ eV}$, in

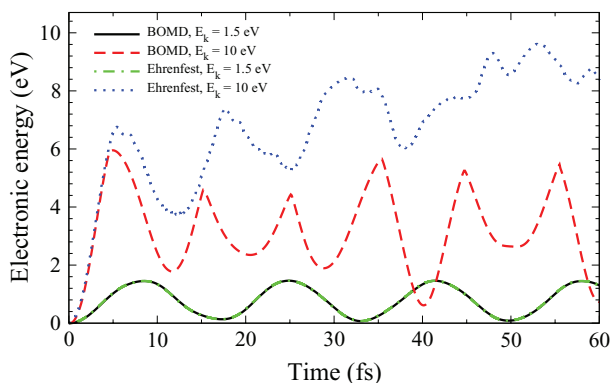


FIG. 2. Time evolution of the PES of the $\text{H}_2\text{C}=\text{NH}_2^+$ molecule. The results obtained with the Ehrenfest MD and the BOMD for low and high initial kinetic energies are compared. In the BOMD simulations, the time step is 0.1 fs. The Ehrenfest MD simulations are performed using the EC force [Eq. (35)] in conjunction with the CG method for calculating the inverse overlap operator.

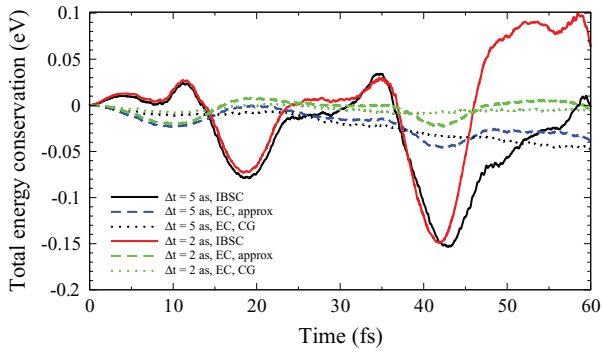


FIG. 3. Conservation of the total energy of the $\text{H}_2\text{C}=\text{NH}_2^+$ molecule as a function of the simulation time. The results obtained with the IBSC and the EC forces [Eqs. (39) and (35), respectively] using two different time steps, $\Delta t = 2$ and 5 as, are compared. The initial kinetic energy of the molecule is $E_k = 10$ eV. Approx and CG correspond to the approximative [Eqs. (49) and (50)] and the CG method for calculating the inverse overlap operator, respectively.

contrast, this is no longer the case. The total energy curves obtained with the different forces and time steps of 2 and 5 as are shown in Fig. 3.

First, we observe that the maximum total energy fluctuation with the IBSC force is roughly the same for both time steps used in the calculations. Second, the EC force in conjunction with the conjugate gradient method for calculating the inverse overlap operator, yields the best total energy conservation for both time steps, $\Delta E_{\text{tot}} = 45$ meV and 9.3 meV for $\Delta t = 5$ and 2 as, respectively. The latter number is very good considering the amount of nonadiabaticity involved in the dynamics, and it could be further improved by decreasing the time step. Furthermore, with $\Delta t = 2$ as, the EC force in conjunction with the approximative inverse already improves the total energy conservation quite significantly compared to the IBSC force. Nevertheless, the error in the total energy is at least twice as high as with the CG inverse.

Next, we study the effect of the grid spacing on the total energy conservation by carrying out simulations with $h = 0.15, 0.2, 0.25$ Å. Because the IBSC force works well with the low initial kinetic energy of $E_k = 1.5$ eV, we only study the more energetic case. The error in the total energy as a function of the grid spacing is presented in Table I.

The accuracy of the approximative inverse increases rapidly as a function of decreasing grid spacing. However, despite the rapid convergence, it is undesirable that the total energy error has such a strong dependence on the grid spacing. In contrast, the grid spacing has very little effect on the results obtained with the CG inverse. For this reason,

TABLE I. Maximum total energy fluctuation of the $\text{H}_2\text{C}=\text{NH}_2^+$ molecule as function of the grid spacing h . The initial kinetic energy is $E_k = 10$ eV. The results obtained with the IBSC and EC forces [Eqs. (39) and (35), respectively] are compared. All the energies are in meV.

h (Å)	$\Delta E_{\text{tot}}^{\text{IBSC}}$	$\Delta E_{\text{tot}}^{\text{EC,approx}}$	$\Delta E_{\text{tot}}^{\text{EC,CG}}$
0.15	148.5	9.95	10.01
0.2	149.19	23.08	9.58
0.25	151.06	228.78	8.86

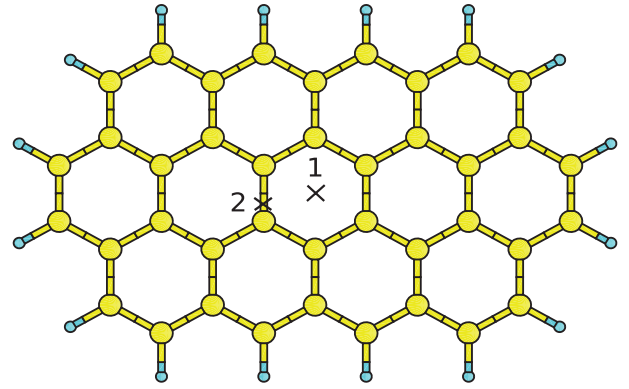


FIG. 4. $\text{C}_{40}\text{H}_{16}$ and the two representative trajectories used in the simulations.

even though the calculations might require, depending on the system, 10%–20% more computational time, the CG inverse should be used for simulations involving nonadiabatic effects instead of the approximative inverse.

C. Hydrogen bombardment of the $\text{C}_{40}\text{H}_{16}$ molecule

As the final test for our PAW-based Ehrenfest MD method, we study the collision of hydrogen with the graphene-like nanoflake $\text{C}_{40}\text{H}_{16}$. With high enough impact energies, the hydrogen projectile will invoke electronic excitations in the target, rendering the BOMD approach unusable. In Ref. 13, a similar hydrogen ion stopping process was studied in the case of graphene, for two representative trajectories: (1) center of hexagon and (2) an impact parameter of 0.25 Å along the C–C bond. The two trajectories are illustrated in Fig. 4.

The EC force in conjunction with the CG method for computing the inverse overlap operator is used in all the calculations. The time step varies between 1 and 5 as such that $\Delta t = 1$ as is used in the simulation with the highest initial projectile energy, $E_k = 10$ keV and $\Delta t = 5$ as in that with the lowest initial energy, $E_k = 100$ eV.

We study the accommodation of the energy transferred into the individual degrees of freedom. Because of the overlap between the augmentation spheres, the PAW method underestimates the atomic forces when the interatomic distance is small. Consequently, we use pair-potential corrections derived from results obtained with FHI-aims (Ref. 35) when the distance between the projectile and the nearest carbon atom is smaller than 0.5 Å. Figure 5(a) shows the total transferred energy and the C recoil energy for the bond trajectory. Electronic excitations significantly influence the results beyond an impact energy of 400 eV as the total transferred energy starts to increase. This observation is in agreement with the Troullier-Martins (TM) pseudopotential-based Ehrenfest MD calculations for graphene in Ref. 13. However, despite the qualitative agreement, the quantitative results differ slightly, which can be attributed to the heavy overlap between the augmentation spheres of the hydrogen projectile and the target carbon atom (see the discussion of Fig. 5(b)). Nevertheless, the agreement is quite good considering that Eqs. (31) and (32) used for

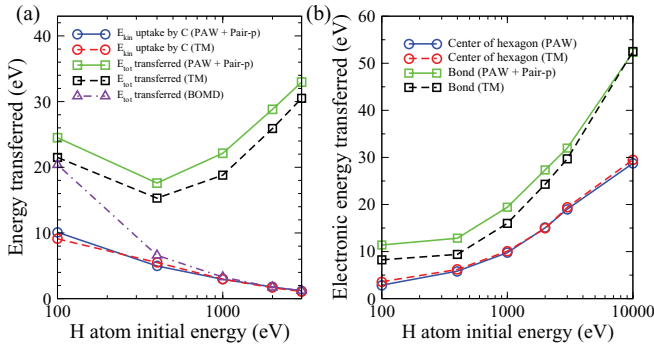


FIG. 5. Deposition of the energy into the individual degrees of freedom in the collision of the H atom with $\text{C}_{40}\text{H}_{16}$. (a) Energy transferred to the target C atom, and the total transferred energy as a function of the H impact energy. The results are shown for the bond trajectory. Pair-p denotes the pair-potential corrections. (b) Energy transferred into the electronic degrees of freedom as a function of H impact energy for both trajectories. The lines are just a guide to the eye.

calculating the \tilde{P} operator are in principle only correct when the augmentation spheres do not overlap.

In Fig. 5(b), the energy transferred into the electronic degrees of freedom is presented. The PAW and TM results are in good agreement for the center of hexagon trajectory, i.e., when there is no overlap between the PAW augmentation spheres. Thus, our method describes electronic excitations in a similar fashion as the TM-based method. Consequently, it seems that our method works correctly in this nonadiabatic case as long as the overlap between the PAW augmentation spheres is not significant. Even in the case of overlapping augmentation spheres, our method can predict qualitative trends with the help of pair-potential corrections.

Finally, we summarize the results regarding the total energy conservation in the calculations. First, in all the simulations for the center of hexagon trajectory, the total energy is conserved to better than 2.7 meV, which is an excellent result considering that the amount of energy deposited into the electronic degrees of freedom is of the order of tens of eV. In the case of the bond trajectory, unfortunately, such good numbers cannot be obtained – the total energy is conserved to better than 230 meV. This is probably due to the breakdown of the zero overlap approximation in deriving the \tilde{P} term as it is essential that this term is correct in order to conserve the total energy. Nevertheless, significant PAW overlap is unusual in Ehrenfest MD applications – the ion bombardment calculation with an impact parameter of 0.25 Å is an extreme case. Thus, in most cases our method can be expected to conserve the total energy very well.

V. CONCLUSIONS

We have described the implementation of the Ehrenfest molecular dynamics within the time-dependent density functional theory and the projector augmented-wave formalism. We have studied the dynamics of small and medium-sized molecules both in adiabatic and in nonadiabatic cases. We found that the incomplete basis set corrected force (Hellmann-Feynman force + Pulay corrections) does not conserve the total energy in nonadiabatic cases, whereas the force

that comes from differentiating the electronic energy (energy-conserving force), conserves the total energy very well as long as the PAW augmentation spheres do not overlap significantly. Finally, the PAW-based Ehrenfest MD results for $\text{C}_{40}\text{H}_{16}$ were compared to Troullier-Martins pseudopotential calculations. From these results, we conclude that our method seems applicable to simulating the nonadiabatic dynamics of medium-sized molecules and beyond as long as the semi-classical and mean-field approximations underlying our method are valid to a reasonable accuracy.

ACKNOWLEDGMENTS

This work has been supported by the Academy of Finland (the Center of Excellence program). The computational time was provided by the Finnish IT Center for Science (CSC) and the Triton cluster of the Aalto School of Science. One of the authors (L. L.) acknowledges the support from the French ANR (ANR-08-CEXC8-008-01). The electronic structure program GPAW is developed in collaboration with CAMd/Technical University of Denmark, CSC, Department of Physics/University of Jyväskylä, Institute of Physics/Tampere University of Technology, and Department of Applied Physics/Aalto University.

APPENDIX: SYMMETRIC FORM OF THE OPERATOR \hat{D}_a

In order to carry out Ehrenfest MD simulations in practice, it is useful to write the \tilde{P} term [Eq. (31)], in a symmetric form reminiscent of the other observables within the PAW method. This can be achieved by deriving a symmetric form for its constituent operator \hat{D}_a [Eq. (32)]. We start by expanding this operator in terms of the PAW projectors and partial waves

$$\begin{aligned} \hat{D}_a &= (1 + \hat{t}_a^\dagger) \frac{\partial \hat{f}_a}{\partial \mathbf{R}_a} = \frac{\partial}{\partial \mathbf{R}_a} \sum_{i_2} (|\phi_{i_2}^a\rangle - |\tilde{\phi}_{i_2}^a\rangle) \langle \tilde{p}_{i_2}^a| \\ &+ \sum_{i_1} |\tilde{p}_{i_1}^a\rangle \langle \phi_{i_1}^a| - \langle \tilde{\phi}_{i_1}^a| \\ &\times \frac{\partial}{\partial \mathbf{R}_a} \sum_{i_2} (|\phi_{i_2}^a\rangle - |\tilde{\phi}_{i_2}^a\rangle) \langle \tilde{p}_{i_2}^a|. \end{aligned} \quad (\text{A1})$$

Rearranging the terms and adding and subtracting a suitable term gives

$$\begin{aligned} \hat{D}_a &= \left(1 - \sum_{i_1} |\tilde{p}_{i_1}^a\rangle \langle \tilde{\phi}_{i_1}^a|\right) \frac{\partial}{\partial \mathbf{R}_a} \sum_{i_2} (|\phi_{i_2}^a\rangle - |\tilde{\phi}_{i_2}^a\rangle) \langle \tilde{p}_{i_2}^a| \\ &+ \sum_{i_1} |\tilde{p}_{i_1}^a\rangle \langle \phi_{i_1}^a| \frac{\partial}{\partial \mathbf{R}_a} \sum_{i_2} (|\phi_{i_2}^a\rangle - |\tilde{\phi}_{i_2}^a\rangle) \langle \tilde{p}_{i_2}^a| \\ &+ \sum_{i_1} |\tilde{p}_{i_1}^a\rangle \langle \tilde{\phi}_{i_1}^a| \frac{\partial}{\partial \mathbf{R}_a} \sum_{i_2} (|\phi_{i_2}^a\rangle - |\tilde{\phi}_{i_2}^a\rangle) \langle \tilde{p}_{i_2}^a| \\ &- \sum_{i_1} |\tilde{p}_{i_1}^a\rangle \langle \tilde{\phi}_{i_1}^a| \frac{\partial}{\partial \mathbf{R}_a} \sum_{i_2} (|\phi_{i_2}^a\rangle - |\tilde{\phi}_{i_2}^a\rangle) \langle \tilde{p}_{i_2}^a|. \end{aligned} \quad (\text{A2})$$

Using the orthonormality of the projectors and pseudo-partial waves, we obtain the following expression:

$$\begin{aligned} \hat{\mathbf{D}}_a = & - \sum_{i_1} |\tilde{p}_{i_1}^a\rangle \langle \phi_{i_1}^a| \frac{\partial}{\partial \mathbf{R}_a} \sum_{i_2} |\tilde{\phi}_{i_2}^a\rangle \langle \tilde{p}_{i_2}^a| \\ & + \sum_{i_1} |\tilde{p}_{i_1}^a\rangle \langle \phi_{i_1}^a| \frac{\partial}{\partial \mathbf{R}_a} \sum_{i_2} |\phi_{i_2}^a\rangle \langle \tilde{p}_{i_2}^a| \\ & + \sum_{i_1} |\tilde{p}_{i_1}^a\rangle \langle \tilde{\phi}_{i_1}^a| \frac{\partial}{\partial \mathbf{R}_a} \sum_{i_2} (|\phi_{i_2}^a\rangle - |\tilde{\phi}_{i_2}^a\rangle) \langle \tilde{p}_{i_2}^a| \\ & - \sum_{i_1} |\tilde{p}_{i_1}^a\rangle \langle \tilde{\phi}_{i_1}^a| \frac{\partial}{\partial \mathbf{R}_a} \sum_{i_2} |\phi_{i_2}^a\rangle \langle \tilde{p}_{i_2}^a|. \end{aligned} \quad (\text{A3})$$

The first term in Eq. (A3) is zero due to orthonormality. Combining the remaining terms then yields the desired symmetric form,

$$\begin{aligned} \hat{\mathbf{D}}_a = & \sum_{i_1, i_2} \left(|\tilde{p}_{i_1}^a\rangle \langle \phi_{i_1}^a| \left. \frac{\partial \tilde{p}_{i_2}^a}{\partial \mathbf{R}_a} \right| + |\tilde{p}_{i_1}^a\rangle \left(\left\langle \phi_{i_1}^a \left| \frac{\partial \phi_{i_2}^a}{\partial \mathbf{R}_a} \right. \right) \right. \\ & \left. \left. - \left\langle \tilde{\phi}_{i_1}^a \left| \frac{\partial \tilde{\phi}_{i_2}^a}{\partial \mathbf{R}_a} \right. \right) \right) \langle \tilde{p}_{i_2}^a|. \end{aligned} \quad (\text{A4})$$

¹R. Car and M. Parrinello, *Phys. Rev. Lett.* **55**, 2471 (1985).

²D. Marx and J. Hutter, *Ab Initio Molecular Dynamics: Basic Theory and Advanced Methods* (Cambridge University Press, 2009).

³J. C. Tully, *J. Chem. Phys.* **93**, 1061 (1990).

⁴K. Yabana and G. F. Bertsch, *Phys. Rev. B* **54**, 4484 (1996).

⁵M. Petersilka, U. J. Gossmann, and E. K. U. Gross, *Phys. Rev. Lett.* **76**, 1212 (1996).

⁶E. Runge and E. K. U. Gross, *Phys. Rev. Lett.* **52**, 997 (1984).

⁷E. Tapavicza, I. Tavernelli, and U. Rothlisberger, *Phys. Rev. Lett.* **98**, 023001 (2007).

⁸J. C. Tully, *Faraday Discuss.* **110**, 407 (1998).

⁹M. Ben-Nun, J. Quenneville, and T. J. Martinez, *J. Phys. Chem.* **104**, 5161 (2000).

¹⁰G. A. Worth, M. A. Robb, and I. Burghardt, *Faraday Discuss.* **127**, 307 (2004).

¹¹C. M. Isborn, X. Li, and J. C. Tully, *J. Chem. Phys.* **126**, 134307 (2007).

¹²Y. Miyamoto, A. Rubio, and D. Tománek, *Phys. Rev. Lett.* **97**, 126104 (2006).

¹³A. V. Krashennnikov, Y. Miyamoto, and D. Tománek, *Phys. Rev. Lett.* **99**, 016104 (2007).

¹⁴L. Blancafort, P. Hunt, and M. A. Robb, *J. Am. Chem. Soc.* **127**, 3391 (2005).

¹⁵N. L. Doltsinis and D. Marx, *J. Theor. Comput. Chem.* **1**, 319 (2002).

¹⁶T. Kunert and R. Schmidt, *Eur. Phys. J. D* **25**, 15 (2003).

¹⁷S. Meng and E. Kaxiras, *J. Chem. Phys.* **129**, 054110 (2008).

¹⁸F. Wang, C. Yung Yam, L. Hu, and G. Chen, *J. Chem. Phys.* **135**, 044126 (2011).

¹⁹O. Sugino and Y. Miyamoto, *Phys. Rev. B* **59**, 2579 (1999).

²⁰X. Andrade, A. Castro, D. Zueco, J. L. Alonso, P. Echenique, F. Falceto, and A. Rubio, *J. Chem. Theory Comput.* **5**, 728 (2009).

²¹P. E. Blöchl, *Phys. Rev. B* **50**, 17953 (1994).

²²M. Walter, H. Häkkinen, L. Lehtovaara, M. Puska, J. Enkovaara, C. Rostgaard, and J. J. Mortensen, *J. Chem. Phys.* **128**, 244101 (2008).

²³B. Walker and R. Gebauer, *J. Chem. Phys.* **127**, 164106 (2007).

²⁴X. Qian, J. Li, X. Lin, and S. Yip, *Phys. Rev. B* **73**, 035408 (2006).

²⁵J. Perdew and S. Kurth, in *A Primer in Density Functional Theory*, edited by C. Fiolhais, F. Nogueira, and M. Marques (Springer-Verlag, 2003), p. 9.

²⁶P. Pulay, *Mol. Phys.* **17**, 197 (1969).

²⁷L. Verlet, *Phys. Rev.* **159**, 98 (1967).

²⁸A. Castro, M. A. L. Marques, and A. Rubio, *J. Chem. Phys.* **121**, 3425 (2004).

²⁹See supplementary material at <http://dx.doi.org/10.1063/1.3700800> for a study of different force expressions for Ehrenfest MD in a one-dimensional position-dependent basis.

³⁰J. J. Mortensen, L. B. Hansen, and K. W. Jacobsen, *Phys. Rev. B* **71**, 035109 (2005).

³¹J. Enkovaara *et al.*, *J. Phys. Condens. Matter* **22**, 253202 (2010).

³²R. Bauernschmitt and R. Ahlrichs, *Chem. Phys. Lett.* **256**, 454 (1996).

³³J. Perdew and Y. Wang, *Phys. Rev. B* **46**, 12947 (1992).

³⁴X. Li, J. C. Tully, H. B. Schlegel, and M. J. Frisch, *J. Chem. Phys.* **123**, 084106 (2005).

³⁵V. Blum, R. Gehrke, F. Hanke, P. Havu, V. Havu, X. Ren, K. Reuter, and M. Scheffler, *Comput. Phys. Commun.* **180**, 2175 (2009).